JACS
JOURNAL OF THE AMERICAN CHEMICAL SOCIETY

Communication

pubs.acs.org/JACS

Gold Nanoclusters Promote Electrocatalytic Water Oxidation at the Nanocluster/$CoSe_2$ Interface

Shuo Zhao,[†] Renxi Jin,[†] Hadi Abroshan,[†] Chenjie Zeng,[†] Hui Zhang,[†] Stephen D. House,[‡] Eric Gottlieb,[†] Hyung J. Kim,[†,§] Judith C. Yang,[‡] and Rongchao Jin*[,†]

[†]Department of Chemistry, Carnegie Mellon University, Pittsburgh, Pennsylvania 15213, United States
[‡]Chemical and Petroleum Engineering, and Physics, University of Pittsburgh, Pittsburgh, Pennsylvania 15261, United States
[§]School of Computational Sciences, Korea Institute for Advanced Study, Seoul 02455, Korea

Supporting Information

ABSTRACT: Electrocatalytic water splitting to produce hydrogen comprises the hydrogen and oxygen evolution half reactions (HER and OER), with the latter as the bottleneck process. Thus, enhancing the OER performance and understanding the mechanism are critically important. Herein, we report a strategy for OER enhancement by utilizing gold nanoclusters to form cluster/$CoSe_2$ composites; the latter exhibit largely enhanced OER activity in alkaline solutions. The Au_{25}/$CoSe_2$ composite affords a current density of 10 mA cm^{-2} at small overpotential of ~0.43 V (cf. $CoSe_2$: ~0.52 V). The ligand and gold cluster size can also tune the catalytic performance of the composites. Based upon XPS analysis and DFT simulations, we attribute the activity enhancement to electronic interactions between nanocluster and $CoSe_2$, which favors the formation of the important intermediate (OOH) as well as the desorption of oxygen molecules over Au_n/$CoSe_2$ composites in the process of water oxidation. Such an atomic level understanding may provide some guidelines for design of OER catalysts.

The oxygen evolution reaction (OER) plays an important role in various energy storage processes and is considered as a major bottleneck of high efficiency electrochemical water splitting for hydrogen fuel generation.[1−4] Owing to the scarcity of current state-of-the-art catalysts (e.g., RuO_2 and IrO_2), cheap cobalt-based materials including oxide, hydroxide, selenide, phosphide, and their derivatives have been extensively explored as alternative OER catalysts;[5−11] however, the inadequate electron conductivity and larger overpotential severely limit their practical application. It has been reported that anchoring gold onto cobalt-based materials can largely improve their OER performance.[12] Several possible reasons have been proposed for explanation of the enhancement by nanogold, including improved electron transfer, synergistic effect, and preferential formation of OOH intermediates.[12c] Until now, the mechanism for the enhancement is still unclear because of the variability and complicacy of the nanogold-loaded composites. Therefore, precise control over morphology and the nanogold component is highly desirable for revealing the mechanistic insight into the nanogold-induced enhancement of OER activity.

Atomically precise gold nanoclusters with tens to hundreds of gold atoms (1 to 2 nm in size) protected by thiolate ligands have attracted significant research interest as a new class of nanomaterials in recent years.[13] Such well-defined $Au_n(SR)_m$ nanoclusters (where n and m represent the numbers of gold atoms and thiolate ligands, respectively) hold promising applications in catalysis, energy conversion, photovoltaics, and sensing.[14−19] A number of atomically precise gold nanoclusters have been synthesized,[20−25] such as $Au_{25}(SR)_{18}$ (1.0 nm gold core diameter), $Au_{144}(SR)_{60}$ (1.7 nm), and $Au_{333}(SR)_{79}$ (2.2 nm), and more importantly, the atom packing structures of some gold nanoclusters have been determined by X-ray crystallography.[13a] As compared with the conventional gold nanoparticles, well-defined gold nanoclusters with crystal structures can serve as model catalysts to achieve atomic level structure−property correlation,[15] providing an opportunity for better understanding of the mechanism in nanocatalysis.

Herein, we utilize the atomically precise $Au_{25}(SR)_{18}$, $Au_{144}(SR)_{60}$, and $Au_{333}(SR)_{79}$ nanoclusters (where R = $-CH_2CH_2Ph$) to construct Au_n/$CoSe_2$ composites for electrocatalytic water oxidation. The Au_n/$CoSe_2$ composites possess high OER activity and durability in alkaline solutions. Based on the molecular precision of $Au_{25}(SR)_{18}$ and its atomic structure, we have provided mechanistic insights into the activity enhancement via a combination of experiment and theory.

The syntheses of $Au_n(SR)_m$ nanoclusters and ultrathin $CoSe_2$ nanosheets followed the previously reported methods (see the Supporting Information for details).[25−28] We first discuss the $Au_{25}(SR)_{18}$ case. The Au_{25}/$CoSe_2$ composite was fabricated by anchoring $Au_{25}(SR)_{18}$ nanoclusters onto $CoSe_2$ nanosheets in dichloromethane under vigorous stirring for 1 h. The composite was collected by centrifugation and then dried under vacuum. The molecular purity of $Au_{25}(SR)_{18}$ has been examined by UV−vis spectroscopy and matrix-assisted laser desorption ionization mass spectrometry (MALDI−MS). Figure 1a shows the UV−vis spectrum of $Au_{25}(SR)_{18}$, in which the peaks at 685, 445, and 400 nm are fingerprints of $Au_{25}(SR)_{18}$ nanoclusters.[27] The X-ray structure of $Au_{25}(SR)_{18}$ (Figure 1a, inset) comprises an icosahedral Au_{13} core protected by six $Au_2(SR)_3$ motifs.[20] Figure 1b shows the MALDI mass spectrum of $Au_{25}(SR)_{18}$ with the molecular ion peak at ~7391 Da (theoretical Mw = 7394,

Received: December 5, 2016
Published: January 9, 2017

DOI: 10.1021/jacs.6b12529
J. Am. Chem. Soc. 2017, 139, 1077−1080

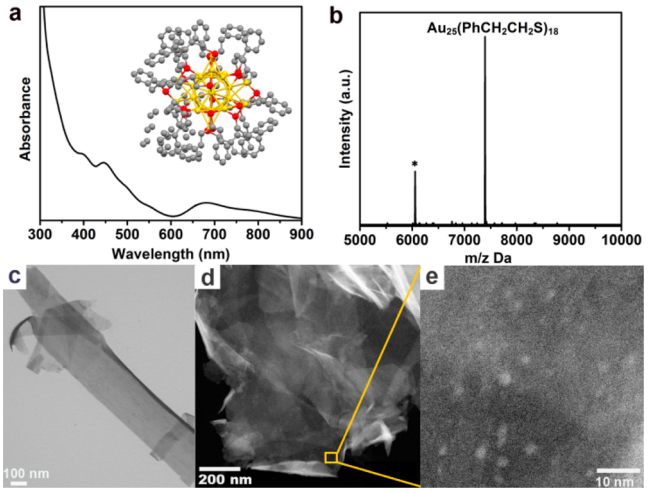

Figure 1. (a) UV−vis and (b) MALDI-MS characterization of $Au_{25}(SR)_{18}$ nanocluster (R = CH_2CH_2Ph). Inset of (a): crystal structure of $Au_{25}(SR)_{18}$ (core diameter: 1 nm). (c) TEM image of $CoSe_2$ nanosheets. (d,e) HAADF-STEM images of $Au_{25}/CoSe_2$ composite with different magnifications.

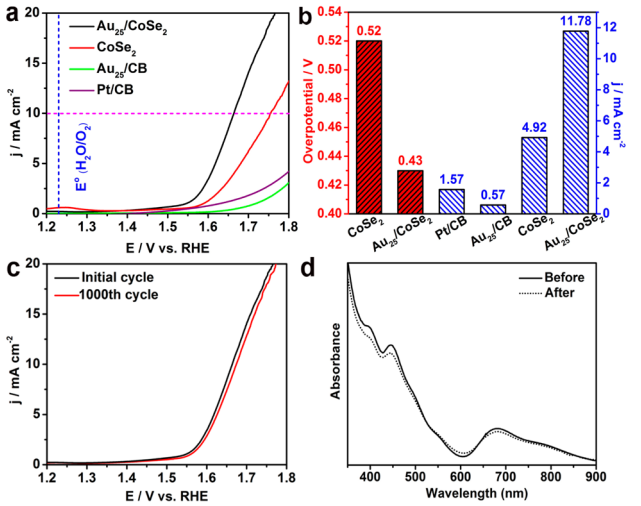

Figure 2. Electrocatalytic performance of the $Au_{25}/CoSe_2$ catalyst. (a) OER polarization curves for $Au_{25}/CoSe_2$, $CoSe_2$, Pt/CB, and Au_{25}/CB. (b) Comparison of the overpotential required for achieving the current density of 10 mA cm^{-2}, and the current density at the overpotential of 0.45 V for $Au_{25}/CoSe_2$, $CoSe_2$, Pt/CB, and Au_{25}/CB catalysts. (c) OER polarization curves for $Au_{25}/CoSe_2$ before and after the stability test. (d) UV−vis spectra of $Au_{25}(SR)_{18}$ nanoclusters before and after the stability test. Catalyst loading: ∼0.2 mg cm^{-2}. Sweep rate: 5 mV s^{-1}. All data were reported without *iR* compensation.

deviation 3 Da) and a fragment at ∼6055 Da (assigned to $Au_{21}(SR)_{14}$). Transmission electron microscopy (TEM) images of $CoSe_2$ nanosheets (Figure 1c and Figure S1a) show the ultrathin sheet structure. The XRD pattern (Figure S1b) reveals the cubic phase (JCPDS 09−0234) of $CoSe_2$ nanosheets. The disappearance as well as broadening of some reflections is attributed to the very thin layer structure of $CoSe_2$ nanosheets.[28] The successful loading of $Au_{25}(SR)_{18}$ onto $CoSe_2$ nanosheets is confirmed by high angle annular dark field scanning transmission electron microscopy (HAADF-STEM) as well as X-ray photoelectron spectroscopy (XPS) analysis. Figure 1d displays a STEM image of $Au_{25}/CoSe_2$, where the small yellow box is magnified in Figure 1e and Au_{25} nanoclusters are well dispersed on the surface of $CoSe_2$ nanosheets. XPS spectra of $Au_{25}/CoSe_2$ composites (Figure S2) show characteristic peaks of Au 4f, further confirming the presence of Au on $CoSe_2$ nanosheets.

We evaluated the OER catalytic performance of $Au_{25}/CoSe_2$ composite in O_2-saturated 0.1 M KOH solution in a standard three-electrode system. The $Au_{25}/CoSe_2$ composite was dissolved in isopropanol and then cast onto glassy carbon working electrode to form a uniform film. Polarization curves were recorded to assess the OER properties. For comparison, similar measurements were also carried out for plain $CoSe_2$ nanosheets and $Au_{25}(SR)_{18}$ nanoclusters supported on carbon black (denoted as Au_{25}/CB), as well as a commercial Pt/CB catalyst. Figure 2a displays the OER polarization curves for $Au_{25}/CoSe_2$, $CoSe_2$, Pt/CB, and Au_{25}/CB, where $Au_{25}/CoSe_2$ exhibits the best OER activity with an early onset potential (∼1.406 V vs RHE) and a high OER current density. Figure 2b compares the OER performance of $Au_{25}/CoSe_2$ with $CoSe_2$, Pt/CB, and Au_{25}/CB. The overpotential (η) corresponding to the current density of 10 mA cm^{-2}, a metric relevant to solar fuel synthesis,[29] is usually considered as a crucial parameter to evaluate the OER properties. Remarkably, the $Au_{25}/CoSe_2$ shows a smaller overpotential (∼0.43 V) than that of plain $CoSe_2$ nanosheets (∼0.52 V), indicating a large enhancement of OER activity after the deposition of $Au_{25}(SR)_{18}$ nanoclusters onto $CoSe_2$ nanosheets. The OER current densities of all three catalysts are also compared at the overpotential of ∼0.45 V (1.68 V vs RHE). $Au_{25}/CoSe_2$ achieves a current density of 11.78 mA cm^{-2} at the overpotential of ∼0.45 V, which is 2.4 times that of $CoSe_2$ nanosheets (4.92 mA cm^{-2}), 7.5 times that of Pt/CB (1.57 mA cm^{-2}), and 20.7 times that of Au_{25}/CB (0.57 mA cm^{-2}). The $Au_{25}/CoSe_2$ catalyst also shows a smaller Tafel slope than the plain $CoSe_2$ nanosheets (Figure S3).

To test the durability of the $Au_{25}/CoSe_2$ catalyst, we applied continuous potential cycling between 0.30 and 0.70 V (vs Ag/AgCl) to the catalyst for 1000 cycles in O_2-saturated 0.1 M KOH solution. Figure 2c shows the polarization curves of $Au_{25}/CoSe_2$ catalyst at the initial cycle and the 1000th cycle. There is a small increase of overpotential (∼11 mV) for $Au_{25}/CoSe_2$ to achieve 10 mA cm^{-2} after 1000 cycles. To further prove the stability of Au_{25} nanoclusters during the OER stability analysis, we directly loaded $Au_{25}(SR)_{18}$ nanoclusters on the glassy carbon working electrode and performed the same potential cycling for 1000 cycles. As shown in Figure 2d, the UV−vis spectra of $Au_{25}(SR)_{18}$ nanoclusters before and after potential cycling exhibit the same characteristic features, indicating the high stability of $Au_{25}(SR)_{18}$ nanoclusters, as was demonstrated in previous electrocatalytic work.[18b,19]

The ligand effect and size dependence were further investigated. We performed thermal annealing treatment of the cluster/$CoSe_2$ composite at 300 °C under N_2 atmosphere for 1 h; of note, the thiolate ligands of $Au_n(SR)_m$ are desorbed at >200 °C.[20] Figure S4 shows a TEM image of the annealed composite, where a larger size distribution of clusters can be observed without ligand protection. Figure 3a shows the OER polarization curves for ligand-on and ligand-off $Au_{25}/CoSe_2$ catalysts in which the ligand removal further improves the OER activity, manifested in the overpotential drop from 0.43 to 0.41 V for 10 mA cm^{-2} and the current density increase from 11.78 to 15.07 mA cm^{-2} at overpotential of 0.45 V (Figure 3b). Such an enhancement in OER performance is attributed to a better interaction between nanogold and $CoSe_2$ nanosheets after ligand removal.

The size of gold nanoclusters was previously found to influence the catalytic activity in thermal hydrogenation

DOI: 10.1021/jacs.6b12529
J. Am. Chem. Soc. 2017, 139, 1077−1080

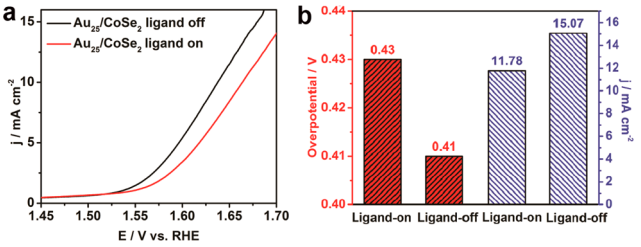

Figure 3. (a) OER polarization curves for ligand-on and ligand-off $Au_{25}/CoSe_2$ catalysts. (b) Comparison of the overpotential (at 10 mA cm^{-2}) and the current density at overpotential of 0.45 V for ligand-on and ligand-off $Au_{25}/CoSe_2$ catalysts. Measurement conditions: see the note in Figure 2.

reaction.[30] To study the potential size dependence for OER, we prepared two larger gold nanoclusters, $Au_{144}(SR)_{60}$ and $Au_{333}(SR)_{79}$, protected by the same phenylethanethiolate ligand as that of $Au_{25}(SR)_{18}$, as well as $Au_{10}(SPh\text{-}^tBu)_{10}$ (see the Supporting Information for synthesis). UV−vis and MALDI-MS were carried out to characterize $Au_{10}(SPh\text{-}^tBu)_{10}$, $Au_{144}(SR)_{60}$, and $Au_{333}(SR)_{79}$ nanoclusters (Figure S5). The $Au_{10}(SPh\text{-}^tBu)_{10}$, $Au_{144}(SR)_{60}$, and $Au_{333}(SR)_{79}$ nanoclusters were respectively loaded onto $CoSe_2$ (all at 2.0 wt %, denoted as $Au_{10}/CoSe_2$, $Au_{144}/CoSe_2$, and $Au_{333}/CoSe_2$). The catalytic performance of $Au_{10}/CoSe_2$, $Au_{144}/CoSe_2$, and $Au_{333}/CoSe_2$ catalysts was tested under the same conditions as $Au_{25}/CoSe_2$. The OER polarization curves are displayed in Figure S6a, which depicts a moderate increase of OER activity with an increase in cluster size. Figure S6b shows the size dependence of overpotential and current density, where the $Au_{333}/CoSe_2$ catalyst possesses the smallest overpotential of ~0.41 V for 10 mA cm^{-2} and the largest current density of 15.44 mA cm^{-2} (3.14 times that of plain $CoSe_2$) at the overpotential of 0.45 V.

It is of major importance to understand the intrinsic reasons of the activity enhancement and the chemistry process of water oxidation. We chose $Au_{25}/CoSe_2$ as a target and conducted XPS analysis to investigate the interactions between $Au_{25}(SR)_{18}$ nanoclusters and $CoSe_2$ nanosheets. As shown in Figure 4a,

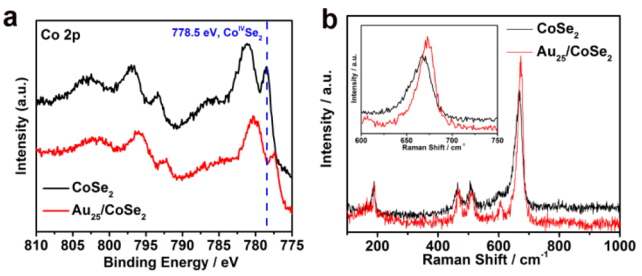

Figure 4. (a) High-resolution Co 2p XPS spectra of plain $CoSe_2$ and the $Au_{25}/CoSe_2$ composite. (b) Raman spectra of plain $CoSe_2$ and the $Au_{25}/CoSe_2$ composite; the inset shows high-resolution Raman spectra.

the electron binding energy of Co 2p in the $Au_{25}/CoSe_2$ composite shows a ~1 eV decrease compared with plain $CoSe_2$, which indicates electronic interaction between $Au_{25}(SR)_{18}$ and $CoSe_2$. Such an electronic interaction is consistent with previous observation in nanogold catalysts.[6a,8,12c] The interaction is also reflected in Raman spectra (Figure 4b) in which four characteristic peaks for cubic $CoSe_2$[31,32] can be found in the Raman spectra of both $CoSe_2$ and the composite. Of note, the Raman peak at ca. 657 cm^{-1} shows a shift toward higher wavenumber after the loading of gold nanoclusters on $CoSe_2$ (inset of Figure 4b), indicating a synergistic electronic interaction between nanocluster and $CoSe_2$, similar to the previous observation in $CeO_2/CoSe_2$.[8,33] Such a synergistic electronic interaction between gold nanoclusters and $CoSe_2$ nanosheets is believed to be valuable for OER enhancement by stabilizing the key hydroperoxy intermediates and optimizing $CoSe_2$/oxygen interactions.[8,12c,34]

Periodic DFT calculations were further performed to provide some general insights into the enhancement of oxygen evolution over systems of nanogold supported on $CoSe_2$ (see computational details in the Supporting Information). We take the following models: (i) a slab of $CoSe_2$ (54 atoms), which is extended in the [210] direction (Figure S7), and (ii) the same slab in which a surface Se atom is replaced with an Au atom (Figure S8). The magnetic properties of the support require extremely expensive spin-polarized calculations. In our preliminary calculations, we simplify Au_{25} as one surface atom in order to reduce computational demanding. Two possible mechanisms *A* and *B* for OER are shown in Figure S9, i.e., mechanism *A* on plain $CoSe_2$ and mechanism *B* on $Au/CoSe_2$. DFT results show that the presence of a gold atom on the $CoSe_2$ surface disfavors the adsorption of hydroxide anion (OH^-) on the catalyst by 0.68 eV/mol ($\Delta\Delta E_A$, Figure S9 and Table S1 in the Supporting Information). Nevertheless, this issue can simply be addressed by increasing the concentration of the base, thereby increasing the chemical potential of free OH^- and hence facilitating its adsorption on the catalyst surface. The formation of intermediate O* with the help of the base (OH^-) is found to be more favorable by 0.21 eV/mol on the Co−Au interface in comparison to Co ($\Delta\Delta E_B$, Table S1). As Figure S9B shows, the coordination number of the intermediate O* on the Co−Au interface is 2, which considerably stabilizes the O*, thereby facilitating its formation on the catalyst surface. Hydroperoxy species (OOH) has been accepted as an important intermediate for oxygen generation.[8,12c] Therefore, effective OER catalysts are expected to favor the formation of OOH, which is unstable and will eventually release the product dioxygen. Although DFT shows the energy change for the formation of OOH is comparable for both model catalysts ($\Delta\Delta E_C$ = 0.05 eV/mol, Figure S9, Table S1), the concentration of the intermediate O* is considerably higher on the Co−Au interface, which in turn speeds up and thus favors the formation of hydroperoxy species (OOH). It is worth pointing out that the as-generated OOH is interacting with both Co and Au sites on the surface; hence, the proton becomes more acidic by 0.19 eV/mol for further abstraction by the OH^- base to form O_2 on the Co−Au interface ($\Delta\Delta E_D$, Figure S9, Table S1). Finally, the as-formed O_2 detaches from the surface to recover the catalytic sites ($\Delta\Delta E_E$, Figure S9, Table S1). This step is found to be more favorable by 0.33 eV/mol on the Co−Au interface than on a Co site of plain $CoSe_2$. This result indicates that incorporating gold clusters onto the $CoSe_2$ catalyst can optimize the Co−oxygen interaction and reduce the undesirable catalyst poisoning caused by exposure to molecular O_2 (the product).

In summary, we have prepared novel Au nanocluster/$CoSe_2$ composites for enhancing the OER properties by utilizing Au_{25}, Au_{144}, and Au_{333} nanoclusters. The $Au_{25}/CoSe_2$ composite displays a much improved overpotential (~0.43 V at current density of 10 mA cm^{-2}) compared to that of plain $CoSe_2$ (~0.52 V), see Table S2 for a comparison with the literature reported nanogold catalysts. Through XPS analysis and DFT calculations, we attribute the activity enhancement to the electronic interaction between Au nanoclusters and $CoSe_2$, manifested in favorable formation of the OOH intermediate and desorption of

DOI: 10.1021/jacs.6b12529
J. Am. Chem. Soc. 2017, 139, 1077−1080

oxygen molecules in the OER process. The Au nanocluster/$CoSe_2$ composites show high stability in alkaline solution. The protecting solutions and nanocluster size can also be utilized to tune the catalytic performance of OER. The gold nanoclusters not only offer deep insights into the catalytic enhancement mechanism at an atomic level but also hold promise in future designing of advanced OER catalysts via combination with other functional materials.

■ ASSOCIATED CONTENT

Supporting Information

The Supporting Information is available free of charge on the ACS Publications website at DOI: 10.1021/jacs.6b12529.

Synthetic and computational procedures, details of electrochemical measurements (PDF)

■ AUTHOR INFORMATION

Corresponding Author

*rongchao@andrew.cmu.edu

ORCID

Chenjie Zeng: 0000-0002-2904-5590
Stephen D. House: 0000-0003-2035-6373
Hyung J. Kim: 0000-0003-4334-1879
Rongchao Jin: 0000-0002-2525-8345

Notes

The authors declare no competing financial interest.

■ ACKNOWLEDGMENTS

R.J. acknowledges support from the Air Force Office of Scientific Research under AFOSR Award No. FA9550-15-1-9999 (FA9550-15-1-0154) and the Camille Dreyfus Teacher-Scholar Awards Program. J.Y. and S.H. acknowledge the financial support of DOE BES through grant DE FG02-03ER15476 and NSF DMREF under contract No. CHE-1534630. This work is also supported in part by the National Science Foundation through NSF Grant No. CHE-1223988 (to H.K.). We thank Joel Gillespie of the University of Pittsburgh Materials Characterization Laboratory (MCL) for access to the XPS spectrometer.

■ REFERENCES

(1) Kumar, A.; Ciucci, F.; Morozovska, A. N.; Kalinin, S. V.; Jesse, S. *Nat. Chem.* **2011**, *3*, 707−713.
(2) Kanan, M. W.; Nocera, D. G. *Science* **2008**, *321*, 1072−1075.
(3) Suntivich, J.; May, K. J.; Gasteiger, H. A.; Goodenough, J. B.; Shao-Horn, Y. *Science* **2011**, *334*, 1383−1385.
(4) (a) Wang, J.; Zhong, H. X.; Qin, Y. L.; Zhang, X. B. *Angew. Chem., Int. Ed.* **2013**, *52*, 5248−5253. (b) Gorlin, Y.; Chung, C.-J.; Benck, J. D.; Nordlund, D.; Seitz, L.; Weng, T.-C.; Sokaras, D.; Clemens, B. M.; Jaramillo, T. F. *J. Am. Chem. Soc.* **2014**, *136*, 4920−4926.
(5) (a) Yeo, B. S.; Bell, A. T. *J. Am. Chem. Soc.* **2011**, *133*, 5587−5593. (b) Han, L.; Yu, X.-Y.; Lou, X. W. *Adv. Mater.* **2016**, *28*, 4601−4605.
(6) (a) Zhang, Y.; Cui, B.; Qin, Z.; Lin, H.; Li, J. *Nanoscale* **2013**, *5*, 6826−6833. (b) Ping, J.; Wang, Y.; Lu, Q.; Chen, B.; Chen, J.; Huang, Y.; Ma, Q.; Tan, C.; Yang, J.; Cao, X.; Wang, Z.; Wu, J.; Ying, Y.; Zhang, H. *Adv. Mater.* **2016**, *28*, 7640−7645.
(7) Liang, L.; Cheng, H.; Lei, F.; Han, J.; Gao, S.; Wang, C.; Sun, Y.; Qamar, S.; Wei, S.; Xie, Y. *Angew. Chem., Int. Ed.* **2015**, *54*, 12004−12008.
(8) (a) Zheng, Y.-R.; Gao, M.-R.; Gao, Q.; Li, H.-H.; Xu, J.; Wu, Z.-Y.; Yu, S.-H. *Small* **2015**, *11*, 182−188. (b) Gao, M.-R.; Cao, X.; Gao, Q.; Xu, Y.-F.; Zheng, Y.-R.; Jiang, J.; Yu, S.-H. *ACS Nano* **2014**, *8*, 3970−3978. (c) Liu, Y.; Cheng, H.; Lyu, M.; Fan, S.; Liu, Q.; Zhang, W.; Zhi, Y.; Wang, C.; Xiao, C.; Wei, S.; Ye, B.; Xie, Y. *J. Am. Chem. Soc.* **2014**, *136*, 15670−15675.
(9) Wu, L.; Li, Q.; Wu, C. H.; Zhu, H.; Mendoza-Garcia, A.; Shen, B.; Guo, J.; Sun, S. *J. Am. Chem. Soc.* **2015**, *137*, 7071−7074.
(10) (a) Chen, P.; Xu, K.; Fang, Z.; Tong, Y.; Wu, J.; Lu, X.; Peng, X.; Ding, H.; Wu, C.; Xie, Y. *Angew. Chem., Int. Ed.* **2015**, *54*, 14710−14714. (b) Mendoza-Garcia, A.; Zhu, H.; Yu, Y.; Li, Q.; Zhou, L.; Su, D.; Kramer, M. J.; Sun, S. *Angew. Chem., Int. Ed.* **2015**, *54*, 9642−9645.
(11) Liu, Y.; Xiao, C.; Lyu, M.; Lin, Y.; Cai, W.; Huang, P.; Tong, W.; Zou, Y.; Xie, Y. *Angew. Chem., Int. Ed.* **2015**, *54*, 11231−11235.
(12) (a) Li, Z.; Ye, K.; Zhong, Q.; Zhang, C.; Shi, S.; Xu, C. *ChemPlusChem* **2014**, *79*, 1569−1572. (b) Zhuang, Z.; Sheng, W.; Yan, Y. *Adv. Mater.* **2014**, *26*, 3950−3955. (c) Liu, X.; Liu, J.; Li, Y.; Li, Y.; Sun, X. *ChemCatChem* **2014**, *6*, 2501−2506.
(13) (a) Jin, R.; Zeng, C.; Zhou, M.; Chen, Y. *Chem. Rev.* **2016**, *116*, 10346−10413. (b) Maity, P.; Xie, S.; Yamauchi, M.; Tsukuda, T. *Nanoscale* **2012**, *4*, 4027−4037. (c) Wang, D.; Padelford, J. W.; Ahuja, T.; Wang, G. *ACS Nano* **2015**, *9*, 8344−8351. (d) Kogo, A.; Sakai, N.; Tatsuma, T. *Nanoscale* **2012**, *4*, 4217−4221.
(14) Sakai, N.; Tatsuma, T. *Adv. Mater.* **2010**, *22*, 3185−3188.
(15) (a) Li, G.; Jin, R. *Acc. Chem. Res.* **2013**, *46*, 1749−1758. (b) Li, G.; Jin, R. *J. Am. Chem. Soc.* **2014**, *136*, 11347−11354.
(16) (a) Kwak, K.; Kumar, S. S.; Lee, D. *Nanoscale* **2012**, *4*, 4240−4246. (b) Kwak, K.; Kumar, S. S.; Pyo, K.; Lee, D. *ACS Nano* **2014**, *8*, 671−679.
(17) Wu, Z.; Wang, M.; Yang, J.; Zheng, X.; Cai, W.; Meng, G.; Qian, H.; Wang, H.; Jin, R. *Small* **2012**, *8*, 2028−2035.
(18) (a) Chen, W.; Chen, S. *Angew. Chem., Int. Ed.* **2009**, *48*, 4386−4389. (b) Lu, Y.; Jiang, Y.; Gao, X.; Chen, W. *Chem. Commun.* **2014**, *50*, 8464−8467.
(19) Kauffman, D. R.; Alfonso, D.; Matranga, C.; Qian, H.; Jin, R. *J. Am. Chem. Soc.* **2012**, *134*, 10237−10243.
(20) Zhu, M.; Aikens, C. M.; Hollander, F. J.; Schatz, G. C.; Jin, R. *J. Am. Chem. Soc.* **2008**, *130*, 5883−5885.
(21) Yamazoe, S.; Takano, S.; Kurashige, W.; Yokoyama, T.; Nitta, K.; Negishi, Y.; Tsukuda, T. *Nat. Commun.* **2016**, *7*, 10414.
(22) Zeng, C.; Chen, Y.; Kirschbaum, K.; Appavoo, K.; Sfeir, M. Y.; Jin, R. *Sci. Adv.* **2015**, *1*, e1500045.
(23) Tang, Z.; Robinson, D. A.; Bokossa, N.; Xu, B.; Wang, S.; Wang, G. *J. Am. Chem. Soc.* **2011**, *133*, 16037−16044.
(24) Negishi, Y.; Sakamoto, C.; Ohyama, T.; Tsukuda, T. *J. Phys. Chem. Lett.* **2012**, *3*, 1624−1628.
(25) Qian, H.; Zhu, Y.; Jin, R. *Proc. Natl. Acad. Sci. U. S. A.* **2012**, *109*, 696−700.
(26) Qian, H.; Jin, R. *Nano Lett.* **2009**, *9*, 4083−4087.
(27) Wu, Z.; Suhan, J.; Jin, R. *J. Mater. Chem.* **2009**, *19*, 622−626.
(28) Gao, M.-R.; Yao, W.-T.; Yao, H.-B.; Yu, S.-H. *J. Am. Chem. Soc.* **2009**, *131*, 7486−7487.
(29) (a) Matsumoto, Y.; Sato, E. *Mater. Chem. Phys.* **1986**, *14*, 397−426. (b) McCrory, C. C. L.; Jung, S.; Peters, J. C.; Jaramillo, T. F. *J. Am. Chem. Soc.* **2013**, *135*, 16977−16987. (c) McCrory, C. C. L.; Jung, S.; Ferrer, I. M.; Chatman, S. M.; Peters, J. C.; Jaramillo, T. F. *J. Am. Chem. Soc.* **2015**, *137*, 4347−4357.
(30) Li, G.; Jiang, D.; Kumar, S.; Chen, Y.; Jin, R. *ACS Catal.* **2014**, *4*, 2463−2469.
(31) Anastassakis, E. *Solid State Commun.* **1973**, *13*, 1297−1301.
(32) Campos, C. E. M.; de Lima, J. C.; Grandi, T. A.; Machado, K. D.; Pizani, P. S. *Phys. B* **2002**, *324*, 409−418.
(33) Yang, C. C.; Li, S. *J. Phys. Chem. B* **2008**, *112*, 14193−14197.
(34) Ogawa, S. *J. Appl. Phys.* **1979**, *50*, 2308−2311.

DOI: 10.1021/jacs.6b12529
J. Am. Chem. Soc. 2017, 139, 1077−1080